

AperTO - Archivio Istituzionale Open Access dell'Università di Torino

**Self-Organisation of Copper Species at the Surface of Cu-TiO<sub>2</sub> Systems During H<sub>2</sub> Evolution Reaction: A Combined Investigation by EPR and Optical Spectroscopy**

**This is a pre print version of the following article:**

*Original Citation:*

*Availability:*

This version is available <http://hdl.handle.net/2318/1768345> since 2021-01-22T16:47:50Z

*Published version:*

DOI:10.1007/s00723-020-01226-w

*Terms of use:*

Open Access

Anyone can freely access the full text of works made available as "Open Access". Works made available under a Creative Commons license can be used according to the terms and conditions of said license. Use of all other works requires consent of the right holder (author or publisher) if not exempted from copyright protection by the applicable law.

(Article begins on next page)

# Self-organisation of copper species at the surface of Cu-TiO<sub>2</sub> systems during H<sub>2</sub> evolution reaction. A combined investigation by EPR and optical spectroscopy.

Alessia Zollo<sup>1</sup>, Valeria Polliotto<sup>1</sup>, Stefano Livraghi<sup>1\*</sup>, Elio Giamello<sup>1</sup>

Department of Chemistry and NIS, University of Torino, Via P. Giuria 7, 10125 Torino, Italy

Corresponding author: Stefano.Livraghi@unito.it

Keywords: Cu<sub>2</sub>O, TiO<sub>2</sub>, EPR, photocatalysis, H<sub>2</sub> evolution

## ABSTRACT.

High surface area TiO<sub>2</sub> was synthesized by means of a solvothermal method and it was then used to prepare two photocatalysts based on copper modified TiO<sub>2</sub>. Two different preparation approaches have been adopted based on the use of the same amount of Cu<sub>2</sub>O (0.5% w/w) as a reactant. The spectroscopic characterization shows that the two preparation procedures lead to distinct distributions of Cu<sub>2</sub>O and other Cu-based species in the final composite materials and that the photoactivity of the solids is strictly related to the nature of the copper species. The joint application of CW-EPR and optical spectroscopy, both employed in catalytic conditions is a sort of “operando” mode, allowed monitoring the evolution of the photocatalytic systems occurring during the H<sub>2</sub> evolution reaction (HER). The effect of water coordination on the Cu(II) species at the surface of titania has been revealed by EPR. The successive photoreduction of the system in the early steps of the photocatalytic reaction involve the reduction of Cu<sup>2+</sup>, the formation of Ti<sup>3+</sup> centres in the oxide matrix and that of metallic copper particles that partially inactivate the system.

## INTRODUCTION

The increased global energy demand and the growing awareness that the exploitation of fossil energy forms inevitably entails adverse effects as global warming and environmental pollution, make H<sub>2</sub> production from water by photocatalytic technologies a strategic research area. Among the various possible approaches heterogeneous photocatalysis is the simplest one and several semiconducting oxides such as those based on TiO<sub>2</sub> (a benchmark material in this field) or on the highly promising SrTiO<sub>3</sub> are currently investigated. All these systems however need, in order to reduce the energy barrier for H<sub>2</sub> formation and to achieve a sustained production of this gas, the presence of co-catalysts or the coupling with other semiconducting materials with suitable band potentials [1-3]. In the search for an optimal co-catalyst for the hydrogen evolution reaction (HER)

the use of earth abundant elements, instead of the efficient but expensive noble metals such as Au and Pt, is considered mandatory. Among the many potentials HER co-catalysts currently under investigation, a class of materials of great importance is represented by copper oxides based systems owing to both their catalytic performance and their relatively low cost. In these systems, copper is often simultaneously present in various forms with different valence state (e.g. metallic copper, dispersed cupric and cuprous ions, cupric or cuprous oxide particles) whose ratio depends, *inter alia*, on the preparation pathway. Due to this high variability in the composition different models, sometime conflicting with each other, were proposed to explain the working mechanism of these co-catalysts [4]. Furthermore, this class of materials suffers of poor stability mainly due to leaching phenomena occurring when they are in contact with aqueous media [5,6]. For this reason, in the recent past several strategies have been also proposed to overcome this drawback including core shell structures [7], protecting coatings [8] or heterojunctions forming Z-scheme [9]. The leaching phenomena are strictly related to the working conditions such as pH, irradiation and so on. The pH of the solution, in particular, plays a crucial role since copper oxides are unstable at acidic pH, and it is worth to mention that, in the case of water photosplitting, the degradation of organic compounds, commonly used as holes scavengers can proceed stepwise, involving stable intermediates such as aldehydes and acids, affecting the pH [2,10]. Another experimental parameter that has an important role in the leaching process is irradiation. V. Gombac et al., for instance, reported that the amount of released  $\text{Cu}^{2+}$  ions is relatively low under irradiation but drastically increases when the powder suspensions are exposed to air in dark condition [11]. Numerous studies have also shown that under irradiation  $\text{Cu}_2\text{O}$  can be easily oxidised into  $\text{CuO}$  due to the accumulation of photogenerated holes ( $\text{h}^+$ ), a process emphasized by the absence of hole scavengers [5]. At the same time numerous works also report, for different Cu containing systems, the formation of metallic copper due to the reduction of the initial Cu species present at the surface of the material [12-14].

Previous work from our research group [4] has shown that the as prepared material simply represents a sort of pre-catalyst that is modified during irradiation leading to the real working systems, and that such a change occurs within few minutes from the start of irradiation. Aim of the present work is the comparison of two photocatalytic systems prepared using the same semiconductor (a nanostructured titanium dioxide synthesized by a solvothermal method showing an exceptionally high surface area) and the same copper compound ( $\text{Cu}_2\text{O}$ ) as starting material for the HER catalyst. In one case a simple grinding of a mechanical mixture of the two oxides was used

(Cu<sub>2</sub>O/TiO<sub>2</sub> sample) while in the second case cuprous oxide was directly added to the reactants of the solvothermal synthesis (CuO<sub>x</sub>/TiO<sub>2</sub> sample). The difference between the two photocatalysts here investigated is related to the procedure used for assembling the two components that leads, as it will be shown in the following, to rather different hybrid systems. The two materials have been investigated coupling Electron Paramagnetic Resonance to classic techniques for solid state analysis focusing the attention on their chemical state and on its transformation during the initial steps of the hydrogen evolution process.

## **MATERIALS and METHODS**

### **1.1. Sample preparation**

TiO<sub>2</sub> was prepared via solvothermal method using ethanol (97%), glycerol and TBT (tetra t-butyl titanate) as precursor of the oxide. In order to favour the TiO<sub>2</sub> crystallization during the solvothermal process 2 ml of water were added into 18 ml of glycerol during stirring, as well as 60 ml of ethanol. Once the system was homogeneous, 2 ml of TBT were added. The solution was stirred for 5 minutes, then transferred into an autoclave and left at 180°C for 24 h. The product was then washed three times with ethanol using a centrifuge to retrieve the solid, and left to dry overnight at 60°C. Hereafter, the material obtained from this procedure will be labelled as "T".

Cu<sub>2</sub>O was prepared by chemical reduction of Cu(II) with glucose according to the Benedict reaction. Cuprous oxide prepared in this way was employed in two methods of deposition on titania (T) leading to two distinct materials labelled Cu<sub>2</sub>O/T, and CuO<sub>x</sub>/T, both having a Cu concentration of 0.5% w/w.

Cu<sub>2</sub>O/T samples were prepared via a prolonged mild grinding in a mortar of the two single powders (T and Cu<sub>2</sub>O). The second material (CuO<sub>x</sub>/T) was obtained adding a weighted amount of Cu<sub>2</sub>O to the autoclave employed for the synthesis of the T sample.

### **1.2. Sample characterization**

*Characterization of the as-Prepared Samples.*

The X-ray diffraction (XRD) powder pattern were recorded with a PANalytical PW3040/60 X'Pert PRO MPD diffractometer using a Cu K<sub>α</sub> radiation source. The diffraction patterns were obtained in the 2θ range between 20° and 80°. The X'Pert High-Score software was used for data handling. The UV-visible diffuse reflectance (DR-UV-vis) spectra of the prepared solids were recorded using a Varian Cary 5000 spectrometer. A poly(tetrafluoroethylene) sample was used as the reference. The

spectra were recorded in the 200–1200 nm range at a scan rate of 240 nm/min with a step size of 1 nm. The measured reflectance was converted with the Kubelka–Munk function.

The specific surface area was measured with a Micromeritics ASAP 2020 apparatus using the Brunauer–Emmett–Teller (BET) model for N<sub>2</sub> adsorption measurements. Prior to N<sub>2</sub> adsorption, the sample was outgassed at 200°C.

Continuous wave electron paramagnetic resonance (CW–EPR) experiments were performed with a Bruker ESP300E spectrometer operating at an X-band (9.5 GHz). All the spectra were recorded under vacuum at 77 K in an EPR cell that can be connected to a conventional high-vacuum apparatus (residual pressure < 10<sup>-4</sup> mbar). In all cases the EPR modulation amplitude was 0.2 mT and the microwave power 10 mW.

High-resolution transmission electron microscopy (HRTEM) images were obtained on a JEOL 3010-UHR instrument (acceleration potential: 300 kV). Samples for TEM investigation were supported onto holed carbon coated copper grid by dry deposition. The FESEM images of the samples were taken using FEG-SEM TESCAN S9000G microscope.

#### *Photocatalytic Test.*

The photocatalytic tests were run on a portion of 30 mg of the photocatalyst suspended in 30 ml of 10% v/v ethanol aqueous solution and sonicated for 2 min. The irradiation source was a 500 W Newport Hg–Xe lamp. A magnetic stirrer was placed at the bottom of the reactor to keep the particles in the suspension during the experiment. Prior to illumination, nitrogen gas was purged into the reactor for 30 min to remove dissolved oxygen. The photocatalytic activity in terms of hydrogen production was then studied by illuminating the suspension for 40 min with the gas sample being taken every 10 minutes. To evaluate hydrogen generation, a GC490 Micro Gas Chromatograph equipped with a MS5A column was used, choosing Ar as gas carrier.

#### *Characterization during H<sub>2</sub> evolution reaction.*

The EPR characterization along the H<sub>2</sub> evolution process was performed by irradiating at room temperature 10 mg of sample, dispersed in 100 μL of water/ethanol solution (10% v/v) and contained in an EPR tube, with a 500 W Newport Hg–Xe lamp. Prior to illumination, the EPR cell was evacuated to remove O<sub>2</sub> while keeping the sample at low temperature to avoid the evaporation of the water/ethanol solution. The experiments were performed stepwise. After each irradiation step, the sample was rapidly frozen from room temperature (RT) to 77 K and transferred to the EPR cavity to record the spectrum. This rapid quenching of the system blocks the photocatalytic process and

the consequent evolution of the catalyst. The adopted procedure can thus be assimilated to an “EPR in operando” methodology. The parameters used for all the EPR spectra were modulation amplitude 0.2 mT and microwave power of 10 mW.

DR-UV-Vis investigations were performed during the H<sub>2</sub> evolution process by irradiating with a 500 W Newport Hg–Xe lamp. The samples were suspended in a water/ethanol solution (10% v/v) in a quartz cell for DR-UV-vis measurements. After irradiation, prior to the spectra acquisition, the samples were allowed to sediment at the bottom of the cell. The DR-UV-vis spectra were recorded in the 250–1200 nm range at a scan rate of 240 nm/min with a step size of 1 nm. Since the samples could not be stirred during irradiation, after every irradiation step the samples were sonicated to disperse the powders homogeneously.

## 2. RESULTS and DISCUSSION

### 2.1. Structure and composition of the prepared samples.

Figure 1 and 2 report the structural and morphological characterization of the three materials prepared in this study. The XRD patterns show that all of them are made up by the sole anatase polymorph. The broad diffraction peaks indicate the nanometric size of the powdered solids. In the case of the Cu<sub>2</sub>O/T sample only (ground mechanical mixture) it is possible to distinguish few diffraction peaks due to Cu<sub>2</sub>O. This indicates that a consistent fraction of the added copper is still present under the form of cuprous oxide crystals, large enough to be detected by XRD, and explains the label (Cu<sub>2</sub>O/T) adopted for this material.

The nanometric nature of the prepared materials is fully confirmed by the TEM images that show primary TiO<sub>2</sub> particles of about 5nm (Fig. 2 A and C) for both copper containing samples. TEM analysis also led to identify in the Cu<sub>2</sub>O/T sample the Cu<sub>2</sub>O particles which are present in the form of small aggregates. Such a distribution finds confirmation also in the FESEM images (Fig. 2 E and F) which made possible the simultaneous investigation of a larger portion of the sample. In agreement with the XRD evidences, also in the TEM/FESEM micrographs of the CuO<sub>x</sub>/T sample no Cu<sub>2</sub>O particles were observed (Fig. 2 B and D) indicating an high dispersion of the copper component in this material.

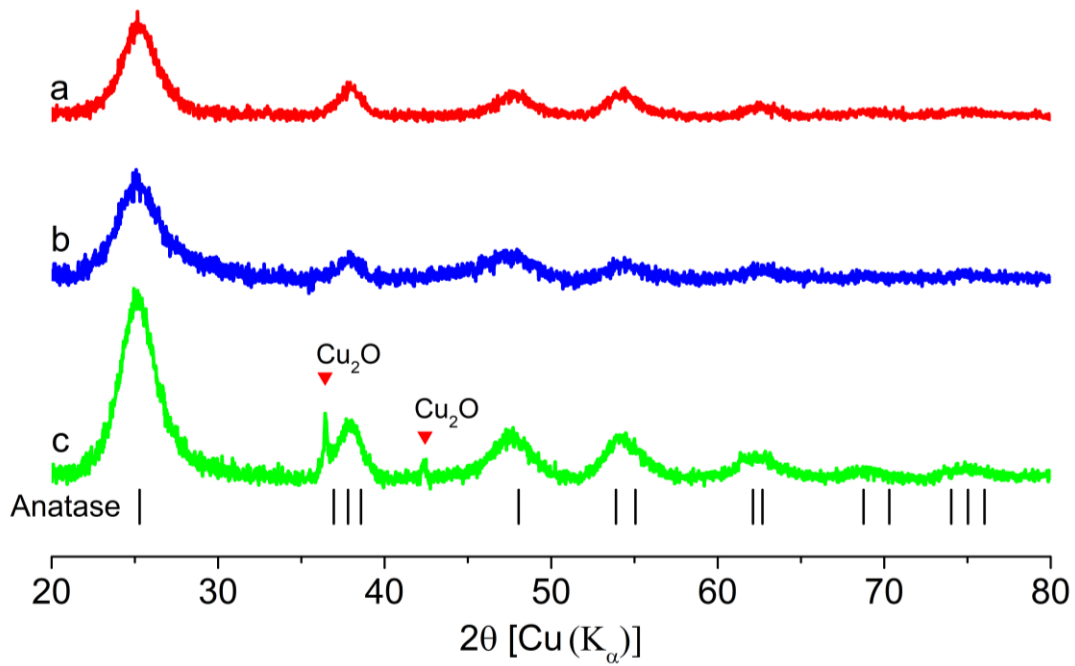


Figure 1: XRD diffractograms of the bare oxide T (a) and the copper modified samples CuOx/T (b) and Cu<sub>2</sub>O/T (c).

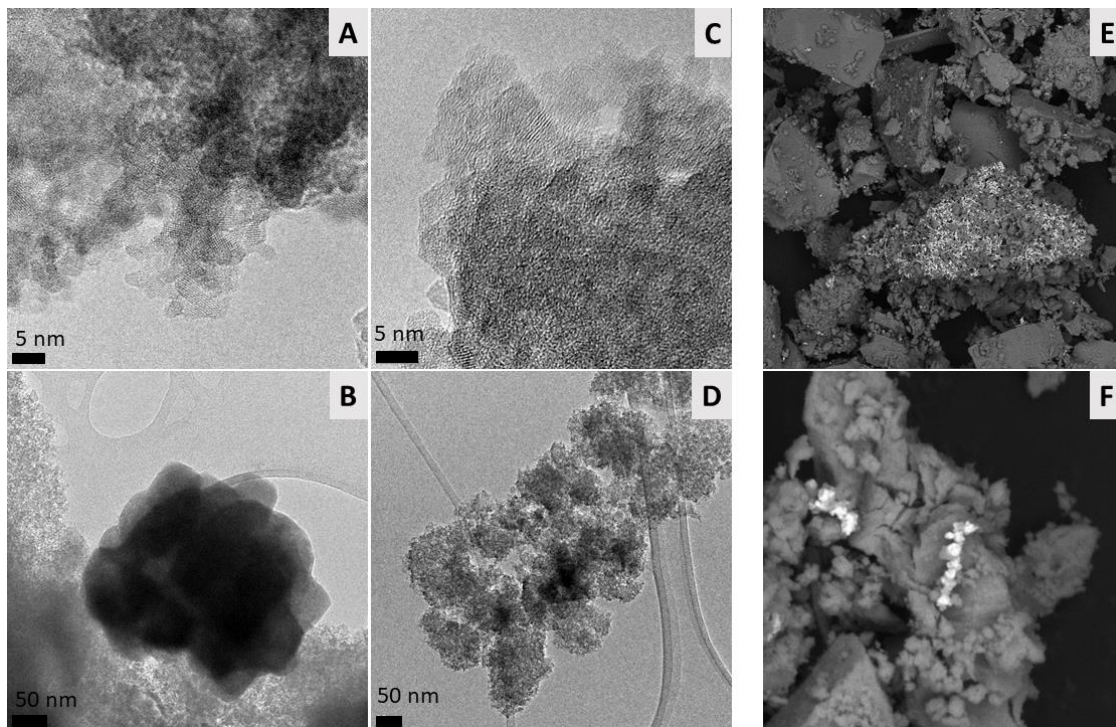


Figure 2: TEM/FESEM micrographs: A, B TEM images of Cu<sub>2</sub>O/T at different magnification. C, D TEM images of CuOx/T at different magnification. E, F FESEM images of Cu<sub>2</sub>O/T, the bright spots are Cu<sub>2</sub>O nanoparticles.

Both photocatalysts show a pinkish colour due to the presence of copper species. Figure 3 shows the optical spectra of the two materials compared with those of the pristine one (T sample). The band gap energy values extracted from these spectra using the Tauc plot method are reported in Table 1.

In both copper containing samples, beside the main absorption due to the band gap transition, further absorptions related to the presence of copper are observed in the 400 - 600 nm region and at higher wavelengths (600 – 1200 nm). The latter is similar for both samples and can be ascribed to the typical d-d transition of Cu(II) species. Such a feature, confirmed by EPR spectra of the as-prepared solids –*vide infra*–, unambiguously indicates that in both cases a fraction of the cuprous oxide has been oxidized and dispersed on the surface of the oxide. As to the signal in the 400 - 600 nm range, the marked difference in intensity and line-shape suggests that the distribution of copper-based species of Cu<sub>2</sub>O/T and CuO<sub>x</sub>/T is somehow different. In agreement with what indicated by X-ray diffraction data and on the basis of the typical optical properties of cuprous oxide, the optical absorption in the range 400 – 600 nm shown by Cu<sub>2</sub>O/T is largely due to the presence of this oxide which is the main, though not the unique, component of the system [15]. The composition of CuO<sub>x</sub>/T is less defined since, neither in by XRD nor by TEM/FESEM microscopies, the starting Cu<sub>2</sub>O or other Cu-containing phases were detected. The observed absorption however is compatible with the presence of both dispersed cuprous ions and of copper oxides (Cu<sub>2</sub>O and CuO) particles whose size however, due to the conditions of the solvothermal treatment, is extremely reduced [16-19]. The EPR signals observed on both as-prepared materials (Figure 4) are due to relatively isolated Cu<sup>2+</sup> ions dispersed at the surface of TiO<sub>2</sub> [4]. Both Cu<sub>2</sub>O and CuO particles are EPR-silent. The amount such Cu<sup>2+</sup> ions is not negligible in both cases but is higher in the case of CuO<sub>x</sub>/T. As mentioned above the presence of surface spread diamagnetic Cu<sup>+</sup> ions cannot be directly confirmed on the basis of the available data but it is absolutely compatible with the observed optical absorption [**Errore. Il segnalibro non è definito.**] and more than probable since the copper phase has undergone a partial dissolution during the preparation as demonstrated by the presence of isolated cupric ions in the system. The joint use of structural, optical and EPR characterization allows therefore a summary description of Cu<sub>2</sub>O/T and CuO<sub>x</sub>/T materials as reported in Table 1 and graphically proposed in Schemes 2A and 2B respectively. The IR spectra recorded for the three materials are practically identical (see spectra in S.I.) indicating that the features of the T support have not been altered by the deposition of the copper co-catalyst.

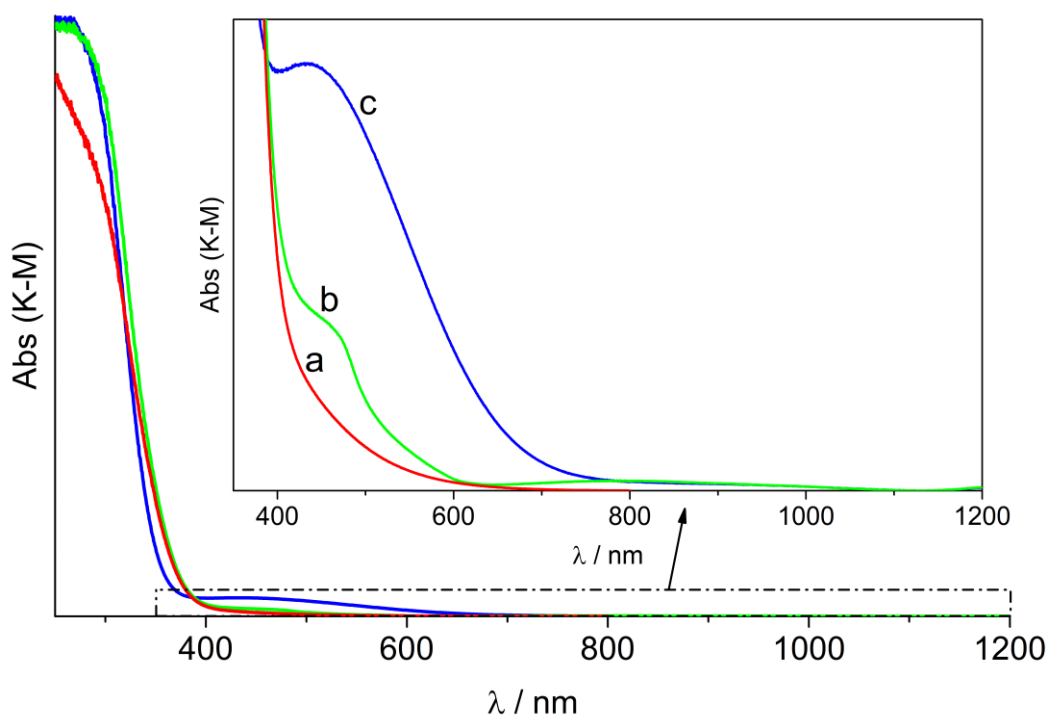


Figure 3: DR-UV-vis spectra of the bare oxide T (a) and the copper modified samples  $\text{Cu}_2\text{O}/\text{T}$  (b) and  $\text{CuO}_x/\text{T}$  (c). The inset reports the magnification of the spectral region between 400-600 nm.

Sample	Phase composition of $\text{TiO}_2$	Crystallite size (nm)	Specific surface area ( $\text{m}^2/\text{g}$ )	Band gap energy $E_g$ (eV)	Nominal Cu content( % w/w Cu)
T	100% anatase	$4.2 \pm 1.1$	/	3.1	0
$\text{Cu}_2\text{O}/\text{T}$	100% anatase	$3.3 \pm 0.9$	373	3.1	0.5
$\text{CuO}_x/\text{T}$	100% anatase	$2.8 \pm 0.7$	464	3.3	0.5

Table1. Main structural and morphological features of the samples investigated in the present work.

## 2.2. Hydrogen evolution test.

Previous work carried out in our research group using different kinds of semiconducting oxides as supports has pointed out that copper species undergo chemical modification during  $\text{H}_2$  evolution reaction, and that these changes were largely accomplished in the first minutes of the process. In order to investigate the behaviour of the materials prepared in the present work, we have followed the photocatalytic activity of the samples in the first 40 minutes of illumination in order to correlate the observed activity with the spectroscopic characterization. Figure 4 compares the  $\text{H}_2$  evolution capability of the copper modified samples with that of the T sample. As expected, the T sample shows a very weak activity compared with that of Cu-modified samples even though the surface

contains carbonaceous species (see IR spectra in SI) that can in principle act as hole scavenger enhancing the H<sub>2</sub> evolution in the initial part of the process. This datum therefore indicates that the role of surface impurities of the support is negligible, and that the increased photocatalytic activity of both mixed materials is exclusively due to the presence of the copper co-catalyst. The observed activity is higher in the case of Cu<sub>2</sub>O/T in all the explored time range pointing to an effect of the presence of relatively large cuprous oxide crystals in the hydrogen evolution reaction, at least in the first catalytic test after preparation.

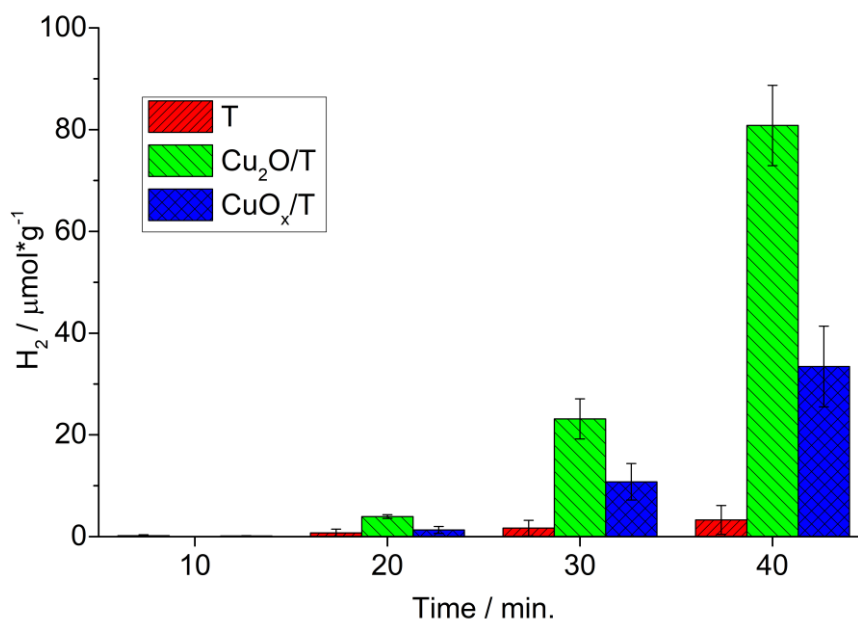


Figure 4: Hydrogen evolution photocatalytic test for the sample T (red), Cu<sub>2</sub>O/T (green) and CuO<sub>x</sub>/T (blue). First cycle after preparation.

The performance of the copper containing photocatalysts as a function of time have been verified repeating four times the H<sub>2</sub> evolution test limited to the first 40 minutes (Fig. 5).

Interestingly the Cu<sub>2</sub>O/T material, more active in the first catalytic cycle (Fig. 4 and 5) loses activity in the successive cycles. At variance CuO<sub>x</sub>/T seems to increase the H<sub>2</sub> production in the second cycle reaching an activity similar to Cu<sub>2</sub>O/T and maintaining this activity also in the third and (partially) in the fourth cycles. Another important notation is that in the first two cycles an induction period is observed between the initial irradiation and a detectable hydrogen production. Both these observations suggest that an evolution of the solid composition and arrangement takes place during the reaction whose analysis, based on spectroscopic technique, will be reported in next Section.

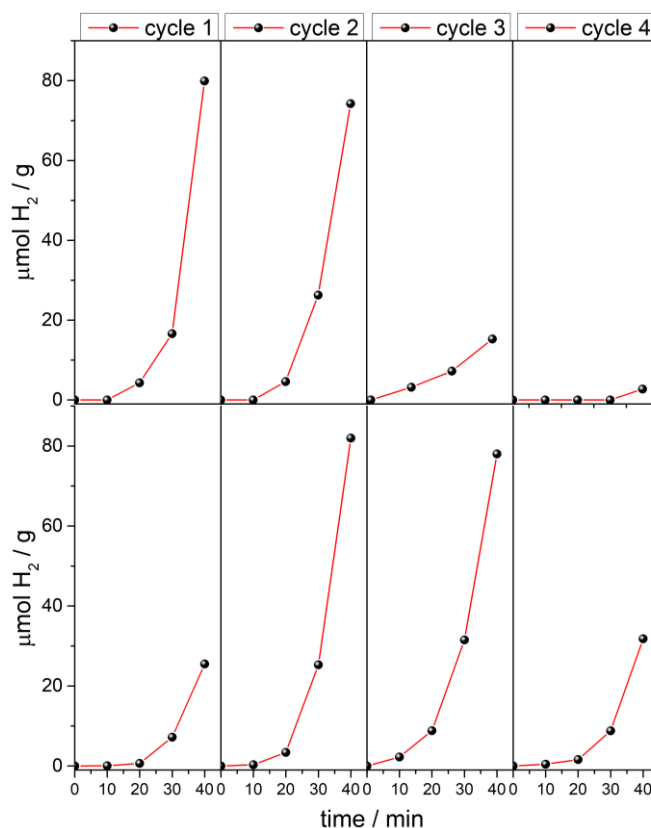


Figure 5. Stability tests for  $\text{Cu}_2\text{O}/\text{T}$  (top) and  $\text{CuO}_x/\text{T}$  (bottom) evaluated monitoring the evolution of  $\text{H}_2$  in four successive photocatalytic cycles.

### 2.3. Cu species at the solid-liquid interface.

Both the as prepared copper modified materials show a CW-EPR signal (black line in Fig. 6) typical of Cu(II) species, more intense in the case of the  $\text{CuO}_x/\text{T}$ . Direct comparison of the spectra show that the EPR signal is the same in the two cases and it is a typical, apparently axial signal due to  $\text{Cu}^{2+}$  ions [20] with the parallel component of the  $\mathbf{g}$  tensor split in 4 hyperfine lines ( $g_{\parallel} = 2.35$  and  $A_{\parallel} = 13.1$  mT) and with unresolved perpendicular component. Similar values are reported for materials containing Cu(II) species on the surface of titanium dioxide [21-23]. The presence of these EPR centres therefore indicates that during the preparation of both  $\text{Cu}_2\text{O}/\text{T}$  and  $\text{CuO}_x/\text{T}$  samples, a fraction of the starting cuprous oxide is oxidized and the resulting  $\text{Cu}^{2+}$  ions are spread on the sample surface. As suggested by the spectra intensity the mechanism of copper dispersion during the preparation is more extended in the case of the sample prepared via solvothermal methods. The dispersion of the dry powders in the water/ethanol solution employed for the  $\text{H}_2$  evolution test instantaneously causes a dramatic change in their EPR spectra. For both samples the signal intensity increases and a shift at higher values of the  $g_{\parallel}$  component is observed while the magnitude of the hyperfine coupling constant  $A_{\parallel}$  remains almost unchanged (red spectra in Fig. 6).

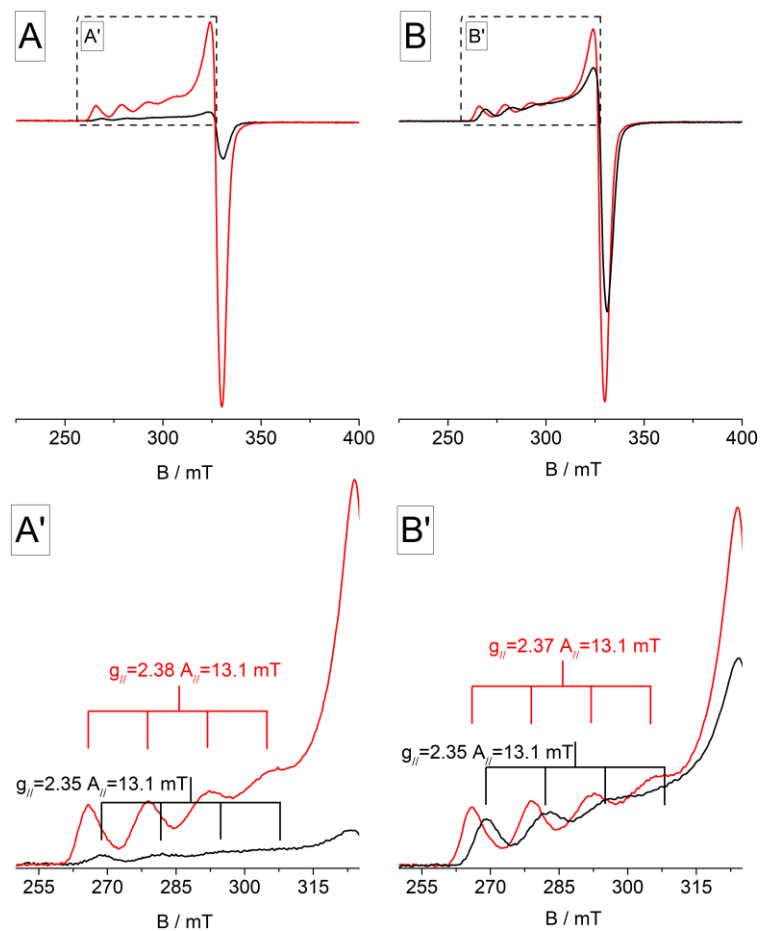


Figure 6: EPR spectra of samples Cu<sub>2</sub>O/T (A) and CuO<sub>x</sub>/T (B) as dry powders (black lines) and dispersed in water/ethanol solution (red lines). In panels A' and B' it is shown the magnification of the areas of interest: in both cases it is evident the shift at higher values of the  $g_{\parallel}$  component after the dispersion in solution, while the hyperfine constant  $A_{\parallel}$  remains unchanged.

In an EPR signal the  $\mathbf{g}$  tensor encodes information about the global symmetry of the electronic distribution. In the present case, a change in the coordination symmetry is expected both in the case of leaching of a fraction of the surface copper that moves from the surface to the solution or in the case of a simple change in the environment of surface anchored Cu<sup>2+</sup> ions due to coordination of water molecules. Both these mechanisms therefore can in principle account for the observed  $g$ -shift. In order to definitively discriminate between the two possibilities, adsorption of water vapour on the dry solid has been performed on both photocatalysts to simulate the effect of contact with the liquid phase (Fig. 7). Upon H<sub>2</sub>O adsorption the observed behaviour is the same for the two solids. The contact with water (20 mbar) induces the same modification observed in suspension: the signal intensity increases, the  $g_{\parallel}$  feature shifts to higher values (from 2.035 to 2.037) while the hyperfine splitting  $A_{\parallel}$  remains constant. Differently from the case of the liquid/solid system however, at the gas/solid interface such a modification takes several hours to be accomplished, probably because

the amount of interacting water molecules is not comparable in the two experimental approaches. It is worth to mention also that the subsequent outgassing of the adsorbed water at RT leads to a recovery of the initial spectroscopic features indicating that the process is reversible even though with different rates in the two cases with  $\text{Cu}_2\text{O}/\text{T}$  (higher amount of dispersed cupric ions) faster than  $\text{CuO}_x/\text{T}$  (Spectra 4 and 5 in Fig.7B).

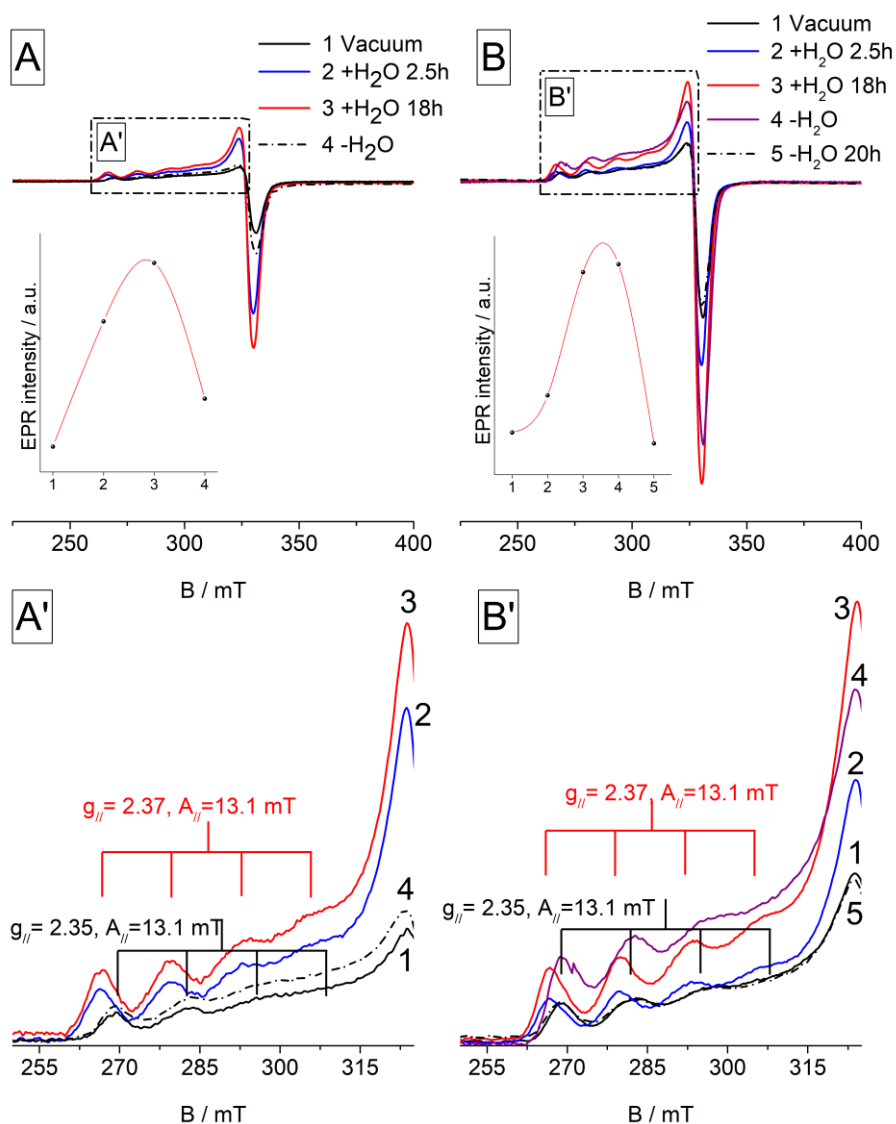


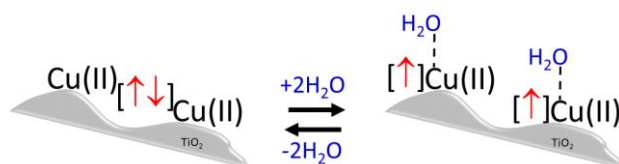
Figure 7: EPR spectra of  $\text{Cu}_2\text{O}/\text{T}$  (A) and  $\text{CuO}_x/\text{T}$  (B) recorded: under vacuum (1, black line), after 2.5 hours under 20 mbar  $\text{H}_2\text{O}$  (2, blue line), after 18 hours under 20mbar  $\text{H}_2\text{O}$  (3, red line), after outgassing and 20 h outgassing (4, 5). Inset: trend of EPR intensity. Panels A' and B' show the magnifications of the spectra to highlight the changes in the  $g_{||}$  region.

The results in Fig. 7 concerning the effect of the aqueous environment on the solid point to an evolution in the coordination sphere of anchored  $\text{Cu}(\text{II})$  species rather than to their leaching in solution. This was conclusively confirmed recording the EPR spectrum of a portion of the liquid phase in contact with the solid in which no signal due to copper ions was observed and checking

also an ad-hoc prepared solution of  $\text{Cu}^{2+}$  in a water-alcohol mixture that shows EPR parameters definitely different from those recorded on the wet solid (See S.I.) [24].

The change in intensity upon wetting therefore implies that new EPR active Cu(II) centres are generated by the coordinative action of water that splits the diamagnetic surface Cu(II) dimers to form EPR active Cu(II) hydrated monomers, since the oxidation of isolated Cu(I) centres by water in the experimental conditions adopted is simply meaningless. The presence of silent Cu(II) dimeric species in fact is well documented in copper containing proteins and it was also reported for Cu containing zeolites [25,26].

The reversibility of the observed process, obtained via simple removal of water by outgassing at room temperature, corroborates this interpretation that is resumed in the picture below reported in which the addition of a water is schematically represented in that the exact number of water molecules entering in the Cu(II) coordination sphere is unknown.

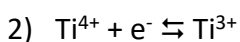
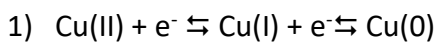


*Scheme 1: Sketch representing the effect of  $\text{H}_2\text{O}$  adsorption on the spin states of a fraction of Cu(II) species.*

Summarizing the evolution of the EPR spectra by contact with the liquid phase is due to the presence of EPR-silent coupled Cu(II) species on the dry, as-prepared material that become EPR-active due to the action of water molecules that split the silent coupled species and enter in the coordination sphere of the isolated cupric ions.

#### **2.4. Cu oxidation states during the $\text{H}_2$ evolution reaction (HER).**

As mentioned in the introduction, an evolution of the co-catalyst phase during the hydrogen evolution reaction has been invoked in the past. The phenomenon is monitored in detail in the present case, as shown in Fig. 8 and Fig. 9. The former figure reports the changes of the EPR features of  $\text{Cu}_2\text{O}/\text{T}$  suspended in ethanol/water solution upon irradiation. The spectra are recorded at regular intervals of 10 minutes. During irradiation of the suspension the intensity of the signals due to Cu(II) hydrated ions progressively decreases and simultaneously a signal of  $\text{Ti}^{3+}$  centres, due to electrons trapped by the  $\text{TiO}_2$  matrix, appears and progressively grows. The observed behaviour indicates that photogenerated electrons are involved in the formation of both reduced forms of copper (Cu(I), Cu(0) *vide infra*) from paramagnetic Cu(II) centres and of  $\text{Ti}^{3+}$  from matrix  $\text{Ti}^{4+}$  ions according to the following reactions [27].



The occurrence, under irradiation, of a true reduction process is further proved by DR-UV-vis spectra obtained in the same described condition (Fig. 9) which are dominated by two main effects, i) the increase of the overall absorption in the region 400-600 nm and, ii) the appearance of a new absorption band at about 575 nm, that gradually increases during the experiment.

The first kind of absorption occurs in the region typical of Cu(I) [19,15] as also indicated by the fact that there is a further increase of the absorption features already present in the as prepared material (Fig. 3 and red line in Fig. 9). The photoreduction process occurring under irradiation is likely based on two processes. These are: i) the formation of isolated Cu(I) species anchored on the TiO<sub>2</sub> surface by direct one-electron reduction of the analogous Cu(II) ones and, ii) the growth of the already present Cu<sub>2</sub>O aggregates or the formation of new nanocrystals of the same oxide. In the second case (ii) migration and aggregation of isolated species are necessary and this likely occurs via leaching of isolated Cu<sup>2+</sup> and Cu<sup>+</sup> species with successive reduction-deposition.

This second feature in Fig. 9 (absorption at about 575 nm) is due to the surface plasmonic resonances (SPRs) of metallic copper nanoparticles indicating that the reduction process described by reaction 1 proceeds until the Cu(0) state [28,29]. A mechanism of leaching-deposition must occur also in this case in order to form metallic aggregates. Inspection of Figure 9 also indicates that this process is faster in the case of the Cu<sub>2</sub>O/T sample where both spectroscopic features are observed after the first 10 minutes of irradiation, whereas for the CuOx/T sample the new absorptions become appreciable only after 30 minutes of irradiation.

Summarizing the joint use of EPR and DR-UV-vis spectroscopy describes a complex surface process based on the photoreduction of Cu(II) surface-anchored hydrated species (very abundant in the material before irradiation) and of analogous Cu(I) species. The whole result is a working HER catalyst that is highly reduced with respect to the starting material and in which Cu<sub>2</sub>O and Cu(0) nanoparticles have a majority role, beside, most likely, isolated surface supported Cu<sup>+</sup> ions.

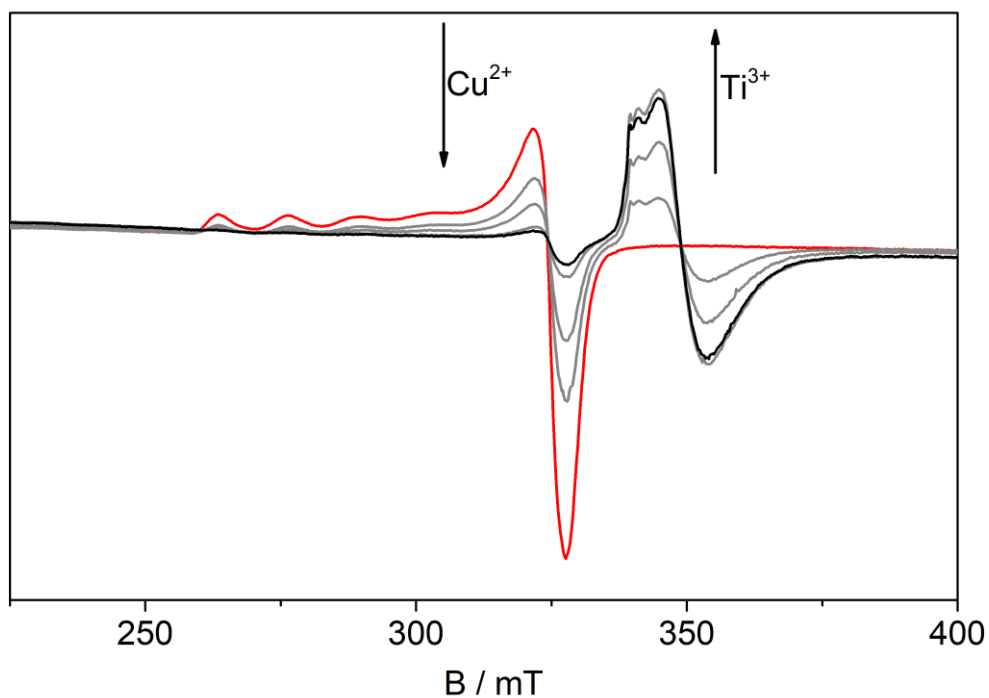


Figure 8: Evolution of the paramagnetic species in the  $\text{Cu}_2\text{O}/\text{T}$  sample dispersed in the ethanol/water solution after irradiation at intervals of 10 minutes. Red line: EPR signal before irradiation; gray lines: spectra recorded after 10, 20 and 30 minutes of irradiation; black line: EPR spectrum after 40 minutes of irradiation.

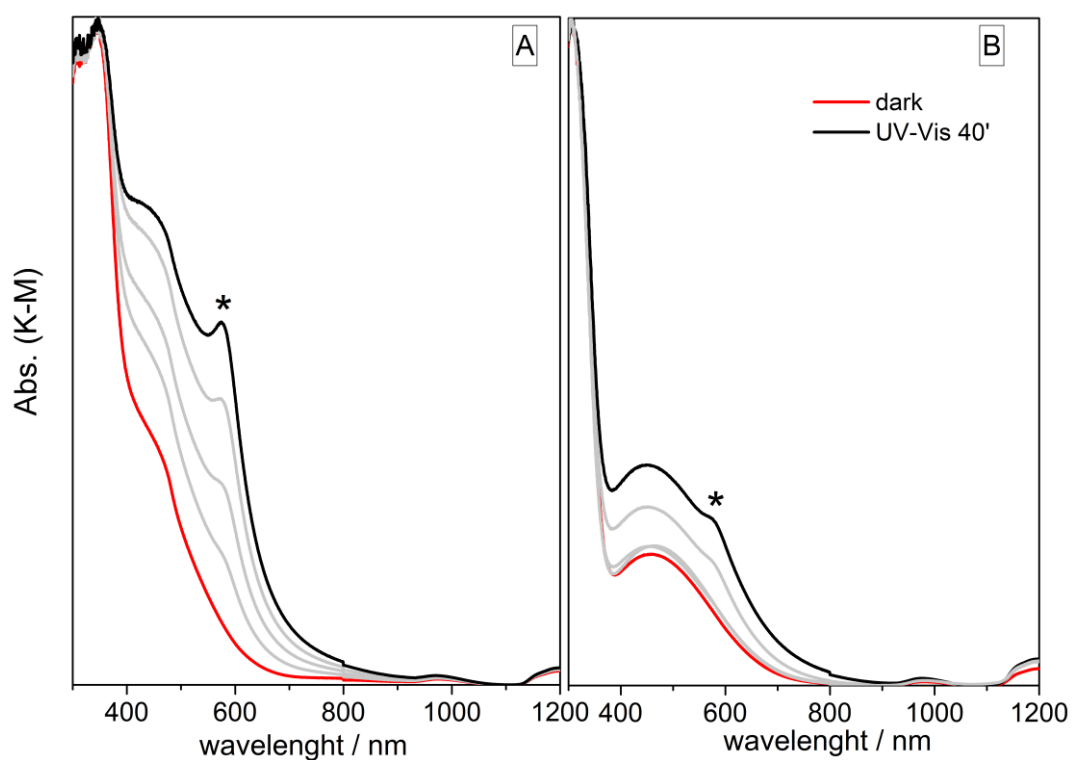
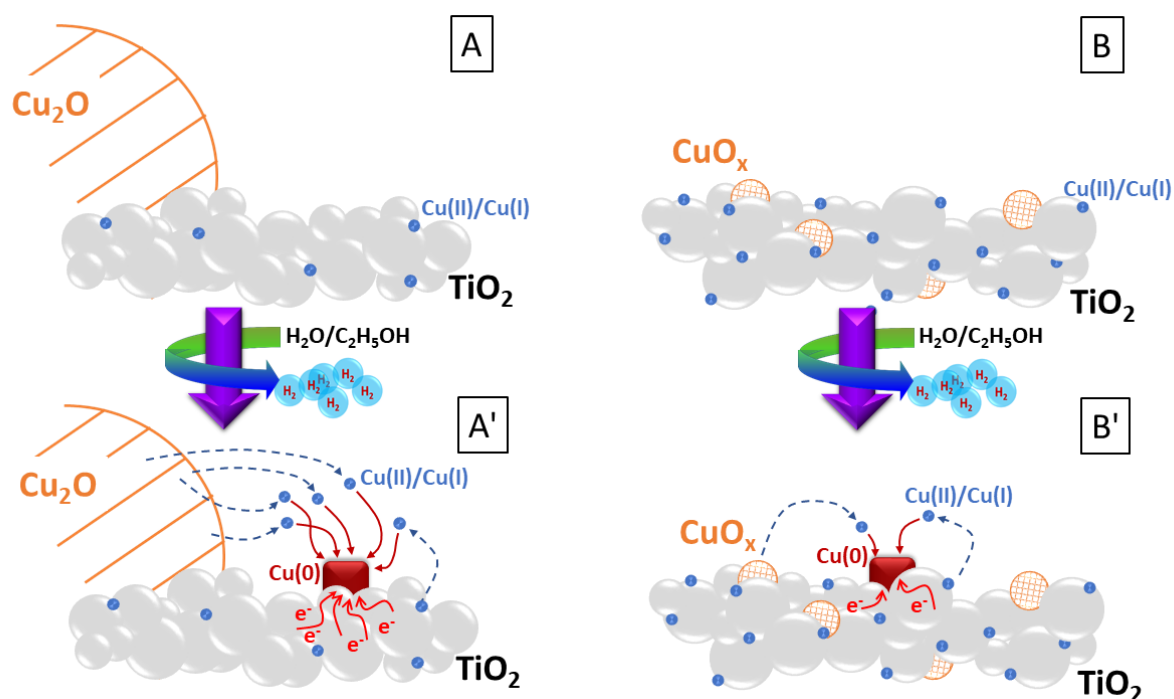


Figure 9: DR-UV-vis spectra under UV-Vis irradiation for  $\text{Cu}_2\text{O}/\text{T}$  (A) and  $\text{CuOx}/\text{T}$  (B). Red line: spectrum in the dark; gray lines: spectra after 10, 20 and 30 min; black line: spectrum after 40 minutes of irradiation. The asterisk identifies the metallic copper plasmonic feature.

## CONCLUDING REMARKS.

Two types of materials based on very high surface area titanium dioxide modified with Cu-based HER co-catalyst have been prepared and tested in the photoproduction of hydrogen. The difference in the photocatalytic activity observed for the two materials relies on the different nature of the copper species present in the system (the copper loading and the TiO<sub>2</sub> material is the same in the two cases) and thus, ultimately, on the procedure followed for the preparation. In both procedures a remarkable oxidation of the cuprous oxide used as reactant occurs leading to the formation of dispersed Cu(II) ions a fraction of which are detected by EPR while a second fraction is under the form of diamagnetic dimers or oligomers which become EPR visible upon contact with the liquid phase without, however, being leached and brought in solution. Dispersed cupric ions are less abundant in the case of Cu<sub>2</sub>O/T that in fact maintains a fraction of copper under the form of Cu<sub>2</sub>O nanocrystals detected by XRD.

In Cu<sub>2</sub>O/T sample, the initial enhancement in HER efficiency with respect to the bare material is due to the p-n junction generated at the Cu<sub>2</sub>O-TiO<sub>2</sub> interface which guarantees an efficient charge carriers separation. In short, upon UV irradiation, because of the potential gradient at the Cu<sub>2</sub>O/TiO<sub>2</sub> interface, the photogenerated electrons migrate from the Cu<sub>2</sub>O to the conduction band of TiO<sub>2</sub> while the photogenerated holes are accumulated in the valence band of Cu<sub>2</sub>O. Errore. Il segnalibro non è definito. In the case of CuOx/T, the initial weaker photoactivity is due to the lower content of Cu<sub>2</sub>O particles reducing thus the beneficial effect of the Cu<sub>2</sub>O-TiO<sub>2</sub> interface. During hydrogen evolution both samples are progressively reduced by photogenerated electrons and the working catalyst contains, beside cuprous oxide and cuprous ions, also copper metal particles that are, at variance with other noble metals such as gold and platinum, detrimental for the catalytic reaction. These reduced species are mainly formed at the expenses of isolated cuprous ions that are first leached from the surface and then deposited in the reduced forms. Simultaneously a partial reduction occurs also in the titanium dioxide matrix that is revealed in terms of the presence of Ti<sup>3+</sup> paramagnetic centres. A tentative drawing reporting the composition of the two systems and their evolution along the of the photocatalytic process is reported in Scheme 2. Practically, no cupric species are present in the working HER catalyst. Despite the initial low photocatalytic activity (Fig. 5), the CuOx/T materials increases its activity in the successive cycles and reach a more stable situation with respect to the sample prepared by grinding (Cu<sub>2</sub>O/T) probably because the higher dispersion of the various copper components limits the formation of metallic particles.



Scheme 2. Cu<sub>2</sub>O/T(A) and CuO<sub>x</sub>/T (B) starting materials and their evolution (A', B') during the photocatalytic reaction.

## Acknowledgements

The FEG-SEM S9000 by Tescan was purchased with funds from Regione Piemonte (project POR FESR 2014-20 INFRA-P SAX).

## References

1. Z. Wang, C. Li, K. Domen, Chem. Soc. Rev. **48**, 2109-2125 (2019)
2. G. L. Chiarello, M.V. Dozzi, E. Selli, J. Energy Chem. **26**, 250–258 (2017)
3. D. Barreca, G. Carraro, V. Gombac, A. Gasparotto, C. Maccato, P. Fornasiero, E. Tondello, Adv. Funct. Mater. **21**, 2611–2623 (2011)
4. V. Polliotto, S. Livraghi, A. Krukowska, M.V. Dozzi, A. Zaleska-Medynska, E. Selli, E. Giamello, ACS Appl. Mater. Interfaces **10**, 27745–27756 (2018)
5. C.Y. Toe, Z. Zheng, H. Wu, J. Scott, R. Amal, Y.H. Ng, Angew. Chem. Int. Ed. **57**, 13613–13617 (2018)
6. X. Chang, T. Wang, P. Zhang, Y. Wei, J. Zhao, J. Gong, Angew. Chem. Int. Ed. **55**, 8840–8845 (2016)
7. Y.-H. Zhang, Y.-L. Li, B.-B. Jiu, F.-L. Gong, J. Chen, S. Fang, H. Zhang, Nanotechnology **30**, 145401 (2019)
8. Z. Zhang, R. Dua, L. Zhang, H. Zhu, H. Zhang, P. Wang, ACS Nano **7**, 1709-0717 (2013)
9. M.E. Aguirre, R. Zhou, A.J. Eugene, M.I. Guzman, M.A. Grela, Appl. Catal. B: Environ. **217** 485–493 (2017)
10. K.-H. Kim, S.-K. Ihm, J. Hazard. Mater. **146** 610–616 (2007)
11. V. Gombac, L. Sordelli, T. Montini, J.J. Delgado, A. Adamski, G. Adami, M. Cargnello, S. Bernal, P. Fornasiero, J. Phys. Chem. A **114**, 3916–3925 (2010)
12. I. Tamiolakis, I.T. Papadas, K.C. Spyridopoulos, G. S. Armatas RSC Adv. **6**, 54848 (2016)
13. G. Li, J. Huang, Z. Deng, J. Chen, Q. Huang, Z. Liu, W. Guo, R. Cao, Cryst. Growth Des. **19**, 5784–5790 (2019)
14. S. Hejazi, S. Mohajernia, Y. Wu, P. Andryskova, G. Zoppellaro, I. Hwang, O. Tomanec, R. Zboril, P. Schmuki, Electrochem. Commun. **98** 82–86 (2019)
15. S. Banerjee, D. Chakravorty, Europhys. Lett. **52**(4), 468-473 (2000)
16. A. Kellersohn, E. Kniizinger, W. Langel, M. Gievsig, Adv. Mater. **7**, 652-655 (1995)
17. W. Cui, W. An, L. Liu, J. Hu, Y. Lian, J. Hazard. Mater. **280**, 417–427 (2014)

18. X. Zou, H. Fan, Y. Tian, M. Zhang, X. Yan, RSC Adv. **5**, 23401-23409 (2015)
19. I. L. Soroka, A. Shchukarev, M. Jonsson, N. V. Tarakina, P. A. Korzhavyi, Dalton Trans. **42**, 9585–9594 (2013)
20. M. Bennati, D.M. Murphy in M. Brustolon, E. Giamello Eds. *Electron Paramagnetic Resonance: a practitioner toolkit*. (John Wiley & Sons Inc. 2009)
21. G. Li, N.M. Dimitrijevic, L. Chen, T. Rajh, K.A. Gray, J. Phys. Chem. C **112** 19040–19044 (2008)
22. Y. Nosaka, S. Takahashi, H. Sakamoto, A.Y. Nosaka, J. Phys. Chem. C **115** 21283–21290 (2011)
23. M. V. Dozzi, G. L. Chiarello, M. Pedroni, S. Livraghi, E. Giamello, E. Selli, Appl. Catal. B: Environ. **209**, 417–428 (2017)
24. W. Burton Lewis, Mohammed Alei Jr., L. O. Morgan, J. Chem. Phys. **45**, 4003 (1966)
25. L. Calabrese, J. Rotilio *Structure and Function of Haemocyanin*, 180-184 (1977)
26. G. T. Palomino, P. Fisticaro, S. Bordiga, A. Zecchina, E. Giamello, C. Lamberti, J. Phys. Chem. B **104**, 4064-4073 (2000)
27. J. Biedrzycki, S. Livraghi, E. Giamello, S. Agnoli, G. Granozzi, J. Phys. Chem. C **118**, 8462–8473 (2014)
28. F. Parveen, B. Sannakki, M. V. Mandke, H. M. Pathan, Sol. Energy Mater. Sol. Cells **144**, 371-382 (2016)
29. M. Singh, I. Sinha, M. Premkumar, A. K. Singh, R. K. Mandal, Colloids Surf. A **359**(1), 88-94 (2010)